Super-Helically Twisted Strands of Poly(*m*-phenylene isophthalamide) (MPDI)

Christian Kübel,*,† Daniel P. Lawrence,‡ and David C. Martin*

Materials Science and Engineering Department, University of Michigan, 2541 Chemistry Building, 930 N. University Avenue, Ann Arbor, Michigan 48109

Received June 11, 2001; Revised Manuscript Received September 7, 2001

ABSTRACT: Low-dose−high-resolution electron microscopy (LD−HREM) was used to analyze the structure of regularly twisted poly(*m*-phenylene isophthalamide) (MPDI) strands formed by slow crystallization from solution. The MPDI chains were found to aggregate into regular assemblies exhibiting uniform twisting at several different length scales ranging from the molecular to the mesoscopic. The MPDI polymer backbone formed a flattened helical structure that was organized into twisted bundles. The helical molecular structure promoted good lateral packing, but led to an open core running down the helical axis, which is presumably filled with solvent and calcium chloride. The electron diffraction and HREM data were consistent with a pseudohexagonal unit cell with $a = b = 1.65 \pm 0.02$ nm, $\gamma = 120 \pm 0.5°$, and $c = 0.378$ nm, where the *c*-axis was oriented nominally parallel to the twist axis of the fiber. The strain induced by the mesoscopic twisting is compensated for by lateral shift disorder between the polymer helices, as confirmed by direct HREM imaging.

Introduction

The structure and properties of biological and synthetic materials are determined by complex molecular and mesoscopic interactions. One of the common structural motifs are helices, which are observed on different length scales ranging from molecular[1−5] to macroscopic.[6−10] On the molecular level, helical structures are highly regular, governed by strong intra- and intermolecular interactions.[3,4,11] On the supramolecular level, the twisting of a meso- or macroscopic assembly is geometrically incompatible with three-dimensional, long-range order of crystalline materials, and thus necessarily involves the formation of defects.[12−14] The competition between twisting and crystallization results in morphologies that depend strongly on chemical structure and processing conditions.[6,15]

Regular meso- or macroscopically twisted structures have been observed for a variety of polymer materials,[7−9,16−18] and different mechanisms for twisting have been proposed.[19−21] Geil and co-workers reported convoluted strands, loops, and toroids in poly(γ-benzyl-L-glutamate), which were sensitive to the processing conditions.[6,22] Li and co-workers reported regularly twisted structures in a synthetic chiral polyester.[7,23] The distortion was characterized as a "double twist", with twisting of the polymer crystal not only around the major axis of the assembly, but along the radial direction as well.

Twisting during crystallization of polymer lamella is intimately linked to banded structures. Its fundamental origin has been related either to enantiomorphic structures or to anisotropic surface forces due to chain-tilt in chain-folded crystals where the molecular stems are not parallel to lamellar normals.[8] On a molecular level, the twisting in polymer lamella is mediated by dislocation arrays perpendicular to the twist axis. However, from a theoretical point of view dislocation arrays parallel to the twist axis have also been considered as a mechanism for twisting (Figure 1).[12,19] The nature of twisting and curvature in polymer crystals has been the subject of a recent review focusing on the defects mediating global distortions of the molecular symmetry and their implications for materials properties.[24]

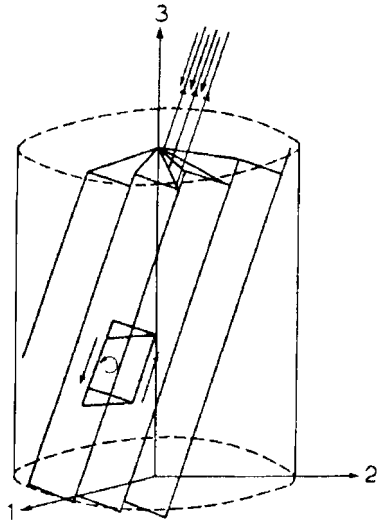

Figure 1. Schematic representation of a twisted fiber according to Bilby and co-workers.[12] The twist mechanism is based on screw dislocations nominally parallel to the twist axis (**3**, vertical). A higher dislocation density is necessary toward the outside of the fiber. Reprinted with permission from ref 12. Copyright 1958 Elsevier.

Here we present detailed studies of an achiral polymer: poly(*m*-phenylene isophthalamide) (MPDI) that spontaneously assembles into regularly twisted helical strands. Low-dose high-resolution electron microscopy

* Corresponding author. Complete address: Department of Materials Science and Engineering and the Macromolecular Science and Engineering Center, The University of Michigan, 2300 Hayward Street, 2022 H. H. Dow Building, Ann Arbor, MI 48109-2136.

† Current address: FEI Company, Achtseweg Noord 5, P.O. Box 80066, 5600 KA Eindhoven, The Netherlands.

‡ Current address: Flint Ink, 4600 Arrowhead Drive, Ann Arbor, MI 48105.

10.1021/ma011016s CCC: $20.00
Published on Web 11/20/2001

(LD−HREM) made it possible to directly image the twisted helical molecular structure, as well as the disorder mediating twisting at a molecular level.

Experimental Section

Materials and Processing. The aromatic polyamide poly(*m*-phenylene isophthalamide) (MPDI), which is commercially available as NOMEX, was obtained from DuPont as a 18 wt% solution in *N*,*N*-dimethylacetamide (DMAc) stabilized by ionic additives (calcium chloride). The MPDI solution was diluted further by DMAc to a concentration of less than 0.1 wt %. This solution was placed in a diffusion vessel, where it was exposed to moisture for a minimum of 3 weeks. A white powder precipitated, which was washed with DMAc and water and kept as a suspension in water. For the TEM sample preparation, a droplet of the suspension was placed on a carbon coated copper TEM grid and the water left to evaporate.

Transmission Electron Microscopy (TEM). A JEOL 2000FX operated at 200 kV was used for TEM bright field imaging of the twisted fibers and recording of selected area electron diffraction (SAED) patterns. A JEOL 4000EX operated at 400 kV (theoretical point-to-point resolution 0.17 nm) was used for the high-resolution electron microscopic analysis.

The SAED patterns were calibrated with respect to gold lattice spacings using gold-coated samples. The room-temperature electron beam stability of the sample (total end-point dose) was determined from the fading of the electron diffraction pattern to be $J_e \sim 0.7$ C/cm^2 at 400 kV. High-resolution images were taken using low-dose conditions[25] at a total dose of 0.09 C/cm^2 (80K magnification, 10 pA/cm^2 beam current on the viewing screen, and 1.4 s exposure time) to ensure that decomposition of the sample did not induce any artifacts.

Digital Image Analysis. The HREM images were digitized for further analysis by scanning the negatives using a LeafScan 45 at a resolution of 5080 dpi. No image rotation or resampling was performed to minimize digital artifacts. Fast Fourier transformations (FFTs) were calculated using the program Scion Image Version Beta 3 by Scion Corp.

Molecular Modeling and Electron Diffraction Simulations. Molecular modeling was performed using Cerius^2 Version 4.0 by Molecular Simulations Inc. with the Dreiding 2.21 force field. A combined approach of energy minimization and NVT anneal dynamics was employed to optimize the molecular geometry. The first few optimization steps were done using the experimental cell parameters as constraints, but the final energy minimization (at high convergence) was performed without any constraints on the unit cell. The molecular structures were used as input for simulating fiber electron diffraction patterns using the diffraction module of Cerius^2. A crystallite size of 200 nm × 200 nm × 1000 nm was assumed with a misorientation of 2°.

Ray-Tracing. The ray tracing program 3D Studio Max by Autodesk/Kinetix was used for simulating the TEM bright-field images of the fibers. The helical models were created with 50% opacity of the material and the reconstruction performed using backlighting.

Results and Discussion

Characterization of the Helical Structure of the MPDI Polymer Fibers at Different Hierarchical Levels. An unusual helical polymer morphology was observed upon slow crystallization of the polyaramide poly(*m*-phenylene diisophthalamide) (MPDI), which is sold commercially by DuPont as dry-spun fibers (NOMEX). Exposure of a dilute (∼0.1 wt %) solution of MPDI in DMAc to moisture over a period of several weeks led to the precipitation of a white powder consisting of aggregates of twisted fibers. The fibers were typically 20−300 nm thick and uniformly twisted over a length of several micrometers. They consisted of one to eight individual strands wrapped around each other forming a periodic multihelical structure similar to a rope (Figure 2). TEM bright-field images of gold shadowed samples indicated about equal numbers of left- and right-handed helices, as would be expected for an achiral polymer.[9]

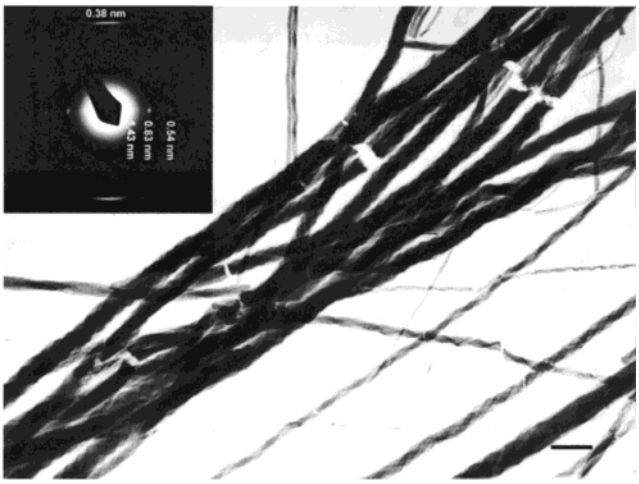

Figure 2. TEM bright-field image of uniformly twisted MPDI fibers consisting of one to eight individual strands (the scale bar represents 500 nm). About equal numbers of left- and right-handed helices have been observed. The inset shows the SAED pattern of one of these fibers indicating their highly ordered structure (the fiber axis is in the vertical direction in this inset).

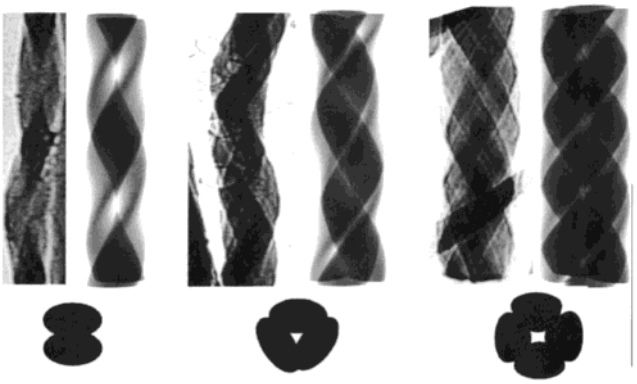

Figure 3. Comparison of TEM bright-field images of fibers consisting of 2, 3, and 4 strands with simulated projections[21] obtained from twisting the basic shapes shown underneath.

The mesoscopic pitch for the individual strands twisting around each other was determined to be 200−1000 nm. The pitch was loosely correlated with the fiber diameter, however there were different twisting modes resulting in a variation of the thickness-to-pitch ratio. The shape and arrangement of the individual strands within one fiber was estimated by comparison of TEM bright-field images with simulated projections of different twisted structures. The best agreement was obtained for slightly distorted elliptical shapes as shown in Figure 3.

Selected area electron diffraction (SAED) of the twisted fibers exhibited a well-defined diffraction pattern indicating a highly ordered microstructure (Inset Figure 2). The observed lattice spacings of the twisted fibers were incompatible with the structure proposed by Kakida et al.[26] for NOMEX (dry-spun MPDI), indicating that the slow crystallization conditions resulted in a new polymorph.

Low-dose high-resolution transmission electron microscopy (LD−HREM)[25] was used to gain a detailed

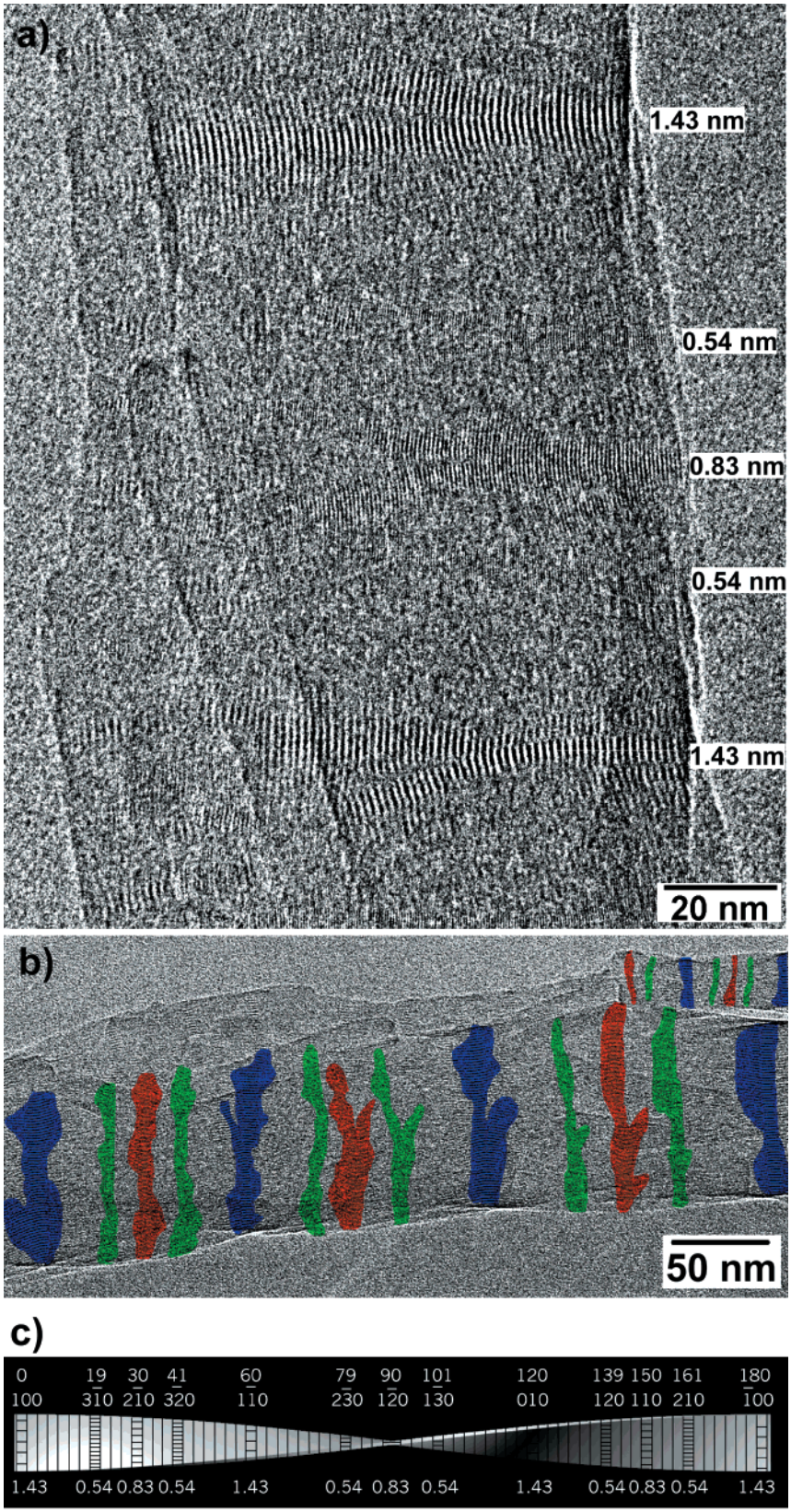

Figure 4. (a) LD−HREM image of a fiber consisting of at least four individual strands. Three different sets of lattice fringes with spacings of 1.43, 0.83, and 0.54 nm are periodically visible in agreement with uniform twisting along the fiber axis. (b) LD−HREM overview image of the same fiber as in part a showing the periodic appearance of the different sets of lattice fringes all the way along the fibber (the areas with the lattice fringes are color coded: blue, 1.43 nm; red, 0.83 nm; green, 0.54 nm). At the right top part a second, thinner fiber is visible, exhibiting a shorter pitch for the different sets of lattice fringes. (c) Schematic drawing showing how uniform twist leads to imaging of different crystallographic zones along the fiber axis.

understanding of the structure and crystallography of the twisted MPDI fibers. The high-resolution images exhibited up to nine different sets of lattice fringes visible as well resolved reflections in the digital FFT. Lattice fringes with spacings of 1.43, 0.83, and 0.54 nm are visible in Figure 4a and corresponded to three

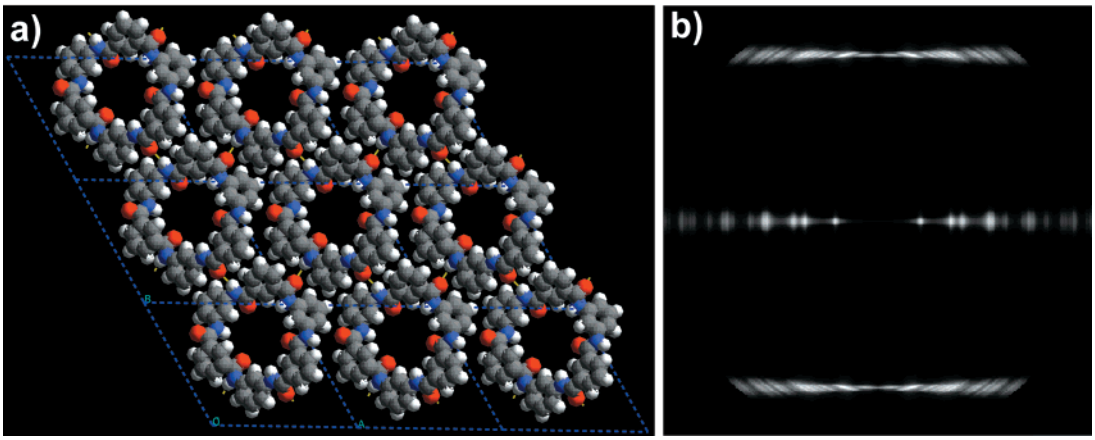

Figure 5. (a) Low-energy model for the polymer conformation in the twisted fibers exhibiting a slightly distorted 3_1 helix viewed along the helix (fiber) axis. (b) Simulated electron diffraction fiber pattern for the model in part a with the fiber (or *c*-axis) in the vertical direction.

different projections of the molecular structure. The periodic appearance of the different sets of lattice fringes along the entire fiber axis (Figure 4b) could be explained by twisting of the crystallographic orientation, resulting in a continuous change of the molecular projection along the fiber axis. The regular periodicity implied a coherent, uniform twist. Each set of lattice fringes was visible all the way across the fiber diameter even though the fibers typically consisted of several individual strands. This indicated that the different strands were in crystallographic registry, presumably related to each other by small angle grain boundaries.

The uniform twist of the crystallographic orientation implied that the distance between different sets of lattice fringes was directly proportional to the angle between the corresponding planes. This information together with the observed lattice spacings was used to determine the unit cell dimensions. An excellent fit with an average error of less than 0.3% was obtained for a pseudohexagonal unit cell with $a = b = 1.65 \pm 0.02$ nm, $\gamma = 120 \pm 0.5°$, and $c = 0.378$ nm, where the *c*-axis was oriented parallel to the twist axis of the fiber (Table 1).

The symmetry and dimensions of the unit cell limited the number of possible molecular conformations, which made a molecular modeling approach feasible to estimate the polymer conformation. The hexagonal symmetry implied that the polymer chains were oriented parallel to the hexagonal axis. However, the unit cell length in this direction was $c = 0.378$ nm and thus only about one-third of the extended monomer length in the commercial MPDI fibers (~1.13 nm).[26] Several attempts with large, high symmetry unit cell structures with extended chains could not satisfactorily explain the electron diffraction pattern, but a model with a helical molecular conformation fit all the known experimental constraints. Molecular modeling resulted in a unit cell exhibiting a slightly distorted 3_1 helix (Figure 5a), which was in excellent agreement with the experimentally determined unit cell dimensions. This model was similar to the helical molecular structures recently proposed by Lehn et al. for a series of *meta*-connected oligo-aramides[27] and also resembled the molecular geometry of the topologically similar *m*-phenylene ethynylene oligomers described by Moore and co-workers.[4,28] The energy calculated for this model was low and as shown by Lehn et al.,[27] the helical conformation not only allows for face-to-face close-packing between the ribbonlike polymer backbones but also allows for favorable hydrogen bonding to residual H_2O or $CaCl_2$ ions that are likely to be present in the open center of the polymer helix. The open helical core of the proposed structure for MPDI is reminiscent of other biopolymers, e.g. poly-(1,4 α-D-glucose) (amylose) found in natural starch that facilitates the well-known formation of stable complexes with iodine.[29] The calculated density using this unit cell ($\rho = 1.32$ g/cm^3) was reasonable and the simulated fiber pattern (Figure 5b) fit well to the experimental electron diffraction patterns (inset Figure 2).

Table 1. Lattice Spacings Observed by LD−HREM Compared to the Reflections Expected for a Hexagonal Crystal Structure with $a = b = 1.65$ nm, $c = 0.378$ nm, and $\gamma = 120°$ [a]

h	*k*	*l*	d_{obs} (nm)	d_{calc} (nm)	Δd (%)	$angle_{obs}$ (deg)	$angle_{calc}$ (deg)
1	0	0	1.43	1.4289	0.08	−3−3	0
1	−1	0	1.43	1.4289	0.08	57−63	60
2	−1	0	0.825	0.825	0	28−33	30
2	0	0	0.715	0.7145	0.08	−3−3	0
2	−2	0	0.715	0.7145	0.08	57−63	60
3	−1	0	0.539	0.5401	0.5	17−22	19
3	−2	0	0.539	0.5401	0.5	39−45	41
3	0	0	0.473	0.4763	0.7	−3−3	0
3	−3	0	0.473	0.4763	0.7	57−63	60
2	−4	0	0.413	0.4125	0.1	28−33	30
4	−1	0	0.398	0.3963	0.4	−*	14
4	−3	0	0.398	0.3963	0.4	−*	46
4	0	0	0.358	0.3572	0.2	−*	0
4	4	0	0.358	0.3572	0.2	−*	60
5	0	0	0.286	0.2858	0.2	−*	0
5	5	0	0.286	0.2858	0.2	−*	60
0	0	1	0.378	0.378	n.a.	0−360	0−360

[a] The experimental lattice spacings were determined from 1024 × 1024 pixel FFTs. The angular range is the average of 5−10 individual observations. [b] These reflections were only observed in the FFT, but the angle could not be measured directly in the image.

As pointed out before, the periodic appearance of the different sets of lattice fringes is the result of systematic twisting of the crystallographic orientation of the fibers. The corresponding "crystallographic" pitch determined by HREM (180−800 nm, proportional to the fiber diameter) did not precisely coincide with the mesoscopic pitch (190−350 nm) for the different strands twisting around each other as determined by bright field TEM (Figure 6). This indicated that there were two different types of supramolecular twisting acting simultaneously for the fibers; the different strands twisting around each other thereby forming a multihelix and, superimposed

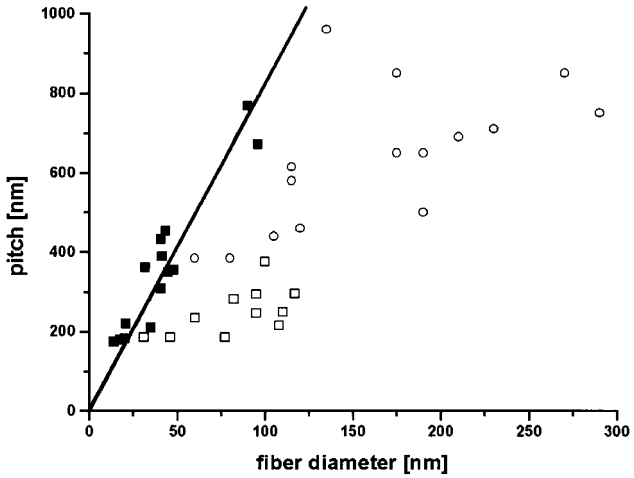

Figure 6. Correlation between the fiber diameter and different twist types: The hollow symbols represent the mesoscopic pitch of the individual strands twisting around each other (two different samples). The filled squares show the crystallographic pitch corresponding to the continuous change of the molecular projection. The linear fit for the crystallographic pitch ($r^2 = 0.90$) corresponds to a constant strain of 7% for a uniformly twisted polymer strand.

on this, the crystallographic twisting of the whole fiber around its long axis. This resulted in a strong rotation of the molecular orientation parallel to the helix axis of up to 2°/nm. Both types of supramolecular twisting were superimposed onto the helical molecular conformation of the polymer chains packed in a hexagonal pattern. This model characterized the structure of the twisted fibers from the molecular dimension to the micrometer range over dimensions of 4 orders of magnitude revealing three hierarchical helical structures.

Shift-Disorder Associated with Uniform Twisting. The uniform supramolecular twisting resulted in path length differences for polymer chains on the inside compared to the outside of each polymer strand. For a typical single stranded fiber with a diameter of 22 nm and a crystallographic pitch of about 180 nm, this corresponded to a strain of about 7%. The strain (ϵ) for a single twisted strand with diameter (D) and crystallographic pitch (p) depends on the diameter-to-pitch ratio according to $\epsilon = l_{\text{outside}}/l_{\text{center}} = \sqrt{1+\pi^2(D/p)^2}$, which is equivalent to $p = \pi/\sqrt{(\epsilon^2-1)}D$. The crystallographic twisting occurs almost uniformly for the whole bundle (not just individually for each strand). The linear dependence of the crystallographic pitch on the fiber diameter indicated that this relationship was a good first approximation even for the multistranded fibers (Figure 6). This strain was accommodated by shift disorder parallel to the molecular axis, as evident from the streaking of the electron diffraction pattern. For the (001) reflection the lateral correlation length corresponded roughly to the helix diameter, implying that each helix was displaced with respect to its neighbors. A similar axial shift disorder has been observed in the rigid-rod polymers PBO and PBZT.[30]

This axial shift disorder evidently mediated the twisting of the helical MPDI molecules and could be directly observed in electron micrographs at high magnifications. Figure 7 shows a small area of a twisted fiber exhibiting the 1.43 nm (100) and 0.54 nm (210) reflections. In addition, there were lattice fringes corresponding to ~0.38 nm ($hk1$) reflections, which were

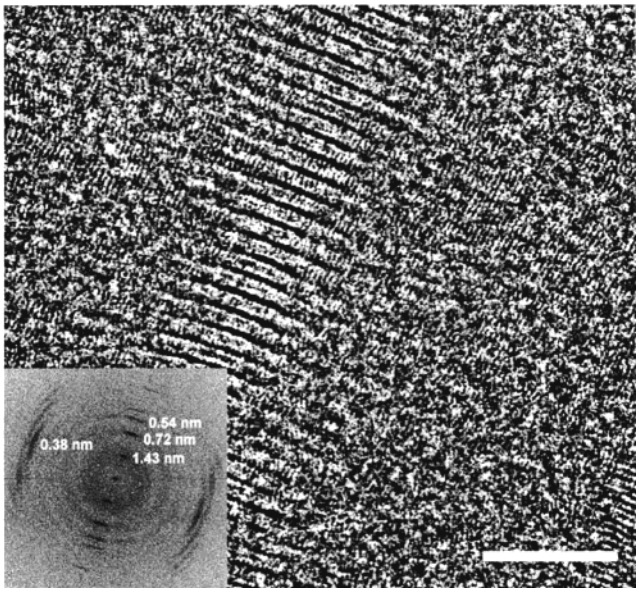

Figure 7. LD−HREM image of a small area of a twisted fiber exhibiting the (001) lattice fringes nominally perpendicular to the 1.43 and 0.54 nm lattice fringes (the space bar corresponds to 10 nm). The wobbling appearance of the (001) lattice fringes can be explained by shift-disorder between neighboring polymer chains. The inset shows the FFT of the HREM image exhibiting a lattice resolution of 0.28 nm. The lattice spacings and the streaking are in good agreement with the electron diffraction data (inset to Figure 2).

nominally perpendicular to the (100) and (210) lattice fringes. These ($hk1$) lattice fringes were visible almost everywhere along the twisted fiber indicating that the twisting did not result in systematic bending perpendicular to the twist direction. However, the high defect density and small d spacings made these lattice fringes sometimes hard to see. They appeared to be wobbling as a result of the shift-disorder between neighboring polymer helices. Nevertheless, the $hk1$ lattice fringes showed a very high correlation along each polymer helix.

Local FFTs of digitized images showed similar streaking as observed in the electron diffraction pattern. This indicated that the structure was best described as an ordered hexagonal columnar liquid crystal with a 2D + 1D order superimposed with a continuous, uniform twist. Compared to the electron diffraction pattern, the local FFT analysis indicated a slightly higher correlation length on the order of a few unit cells. Nevertheless, the reduced dimensionality evidently resolved the geometrical incompatibility between uniform twist and a periodic crystalline structure similar to the "bundles of pencils" model predicted by Bilby[12] and the "twisted rope" model by Lubensky and co-workers.[19] The localization of the deformation presumably corresponds to screw dislocations parallel to the axis of twist. To our knowledge, this is the first time that this twisted mesophase with axial shift-disorder has been observed experimentally. The direct imaging of this shift disorder (Figure 7) gives new insight about the relationship between crystalline order and continuous mesoscopic deformations.

A detailed understanding of the physical origin of the experimentally observed twisting remains elusive. However, our modeling results showed evidence for symmetry breaking of the regular helix that may be involved in this process. In a regular helix, the position of the individual repeat units projected onto the helix axis

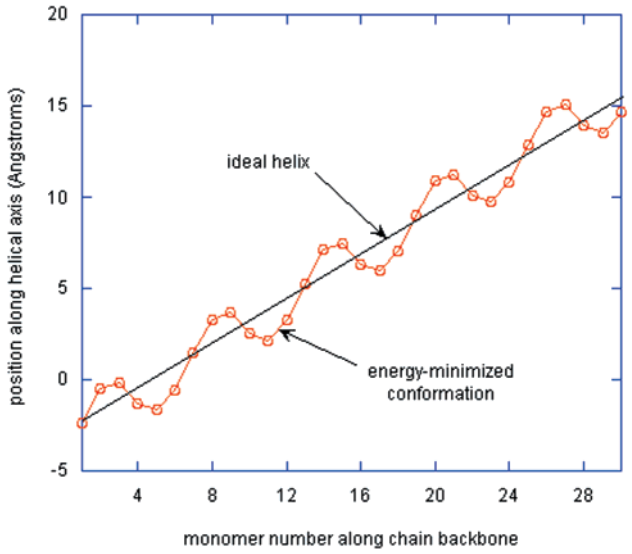

Figure 8. Projection of the position of monomer units in the MPDI polymer backbone onto the helix axis. The position corresponds to the unique carbon atom in the aromatic rings located between either the carbonyl or the −NH units. In the proposed helical conformation of MPDI these atoms are all on the inside of the helix. The backbone conformation of the optimized molecular model (circles) is slightly distorted from that of an ideal helix (straight line).

changes continuously as one moves along the chain backbone. In Figure 8 we plotted the projection of the polymer backbone onto the helix axis, and found that the optimized conformation was distorted away from a pure helix. It may be that the lateral interactions that arise from this flattening led to the formation of a distortion that initiated the supramolecular twisting. Of course, any such mechanism would need to induce these distortions in a systematic, continuous way, since there is little or no evidence for regular faceting on the external surface of fiber bundles.

Conclusions

The results of our LD−HREM study of these superhelical MPDI polymer fibers show that the fibers exhibit several levels of helical structures from the molecular to the macroscopic. The LD−HREM images directly revealed the full structure of these complex macroscopic objects at molecular resolution, and enabled us to study the relationship between molecular interactions and meso- and macroscopic structure. In the current case, we propose that the macroscopically observed twisting reflects the fact that the polymers themselves are locally packed into flattened, distorted helices and that this twisted structure is maintained in the structure as a whole as subsequent helices are deposited onto the growing surfaces. This materials system may serve as a model for the formation of a complex macroscopic structure from molecular entities, which might help to improve the understanding of meso- and macroscopic structural principles in molecular biology and biomimetics.

Acknowledgment. C.K. thanks the Alexander-von-Humboldt (AvH) Foundation and the German Bundesministerium für Bildung und Forschung for a postdoctoral fellowship. D.C.M. thanks the National Science Foundation (NSF) and the AvH Foundation for financial support. The authors gratefully acknowledge helpful discussions with Dr. Kenncorwin H. Gardner of the DuPont Central Research and Development laboratories.

References and Notes

(1) Watson, J. D.; Crick, F. H. *Nature* **1953**, *171*, 737.
(2) Friedman, A. M.; Fischmann, T. O.; Steitz, T. A. *Science* **1995**, *268*, 1721.
(3) Dickerson, R. E. *Methods Enzymol.* **1992**, *211*, 67.
(4) Sherman, M. B.; et al. *J. Mol. Biol.* **1997**, *120*, 245.
(5) Mio, M. J.; Prince, R. B.; Moore, J. S.; Kuebel, C.; Martin, D. C. *J. Am. Chem. Soc.* **2000**, *122*, 6134.
(6) Rybnikar, F.; Geil, P. H. *Biopolymers* **1972**, *11*, 271.
(7) Li, C. Y.; Cheng, S. Z. D.; He, J. J.; Bai, F.; Zhang, J. Z.; Mann, I. K.; Harris, F. W.; Chien, L.-C.; Lotz, B. *Phys. Rev. Lett.* **1999**, *83*, 4558.
(8) Keith, H. D.; Padden, F. J., Jr. *Macromolecules* **1996**, *29*, 7776.
(9) Lawrence, D. P.; Martin, D. C.; Jiang, T. *Polym. Prepr.* **1997**, *345*.
(10) Yang, H.; Coombs, N.; Ozin, G. A. *Nature* **1997**, *386*, 692.
(11) Gorin, A. A.; Zhurkin, V. B.; Olson, W. K. *J. Mol. Biol.* **1995**, *247*, 34.
(12) Bilby, B. A.; Gardner, L. R. T.; Smith, E. *Acta Metall.* **1958**, *6*, 29.
(13) Nye, J. *Acta Metall.* **1953**, *1*, 153.
(14) Yang, H.; Ozin, G. A.; Kresge, C. T. *Adv. Mater.* **1998**, *10*, 883.
(15) von Berlepsch, H.; et al. *J. Phys. Chem. B.* **2000**, *104*, 5255.
(16) Akizuki, T.; et al. *Jpn. J. Appl. Phys.* **1999**, *38*, 4832.
(17) Dierking, I.; Lagerwall, S. T. *Liq. Cryst.* **1999**, *26*, 83.
(18) Chen, X.; Motojima, S. *J. Mater. Sci.* **1999**, *34*, 5519.
(19) Lubensky, T. C.; Harris, A. B.; Kamien, R. D.; Yan, G. *Ferroelectrics* **1998**, *212*, 1.
(20) Kamien, R. D.; Nelson, D. R. *Phys. Rev. E.* **1996**, *53*, 650.
(21) Podgornik, R.; Žekš, B. *Phys. Rev. Lett.* **1998**, *80*, 305.
(22) Blais, J. J.; Geil, P. H. *J. Ultrastruct. Res.* **1968**, *22*, 303.
(23) Li, C. Y.; Yan, D.; Cheng, S. Z. D.; Bai, F.; He, T.; Chien, L.-C.; Harris, F. W.; Lotz, B. *Macromolecules* **1999**, *32*, 524.
(24) Kübel, C.; Gonzalez-Ronda, L.; Drummy, L. F.; Martin, D. C. *J. Phys. Org. Chem.* **2000**, *13*, 816.
(25) Martin, D. C.; Thomas, E. L. *Polymer* **1995**, *36*, 1743.
(26) Kakida, H.; Chatani, Y.; Tadokoro, H. *J. Polym. Sci.* **1976**, *14*, 427.
(27) Berl, V.; Huc, I.; Khoury, R. G.; Krische, M. J.; Lehn, J.-M. *Nature* **2000**, *407*, 720.
(28) Prince, R. B.; Saven, J. G.; Wolynes, P. G.; Moore, J. S. *J. Am. Chem. Soc.* **1999**, *121*, 3114.
(29) Calabrese, V. T.; Khan, A. *J. Polym. Sci., Polym. Chem.* **1999**, *37*, 2711.
(30) Martin, D. C.; Thomas, E. L. *Macromolecules* **1991**, *24*, 2450.

MA011016S